

Supplementary material for
**Intraseasonal to interannual variability of
zooplankton biomass and standing stock inferred
from ADCP backscatter in the eastern Arabian Sea**

R. K. Sahu^{1,2}, D. Shankar^{1,2,*}, P. Amol^{1,3}, S. G. Aparna^{1,2}, D. V. Desai^{1,2}

¹*CSIR National Institute of Oceanography, Dona Paula, Goa-403004, India.*

**Corresponding author (Email: shankar@nio.res.in)*

²*Academy of Scientific and Innovative Research (AcSIR), Ghaziabad, 201002,
Uttar Pradesh, India*

³*CSIR-NIO, Regional Centre, Visakhapatnam, 530017, Andhra Pradesh, India*

- 1 The supplementary material consists of a detailed comparison with biomass climatology
2 from (Aparna et al., 2022) (henceforth, A22). A brief introductory section about com-
3 ponents of seasonal cycle and variabilities followed by overview of analysis tools used to
4 identify the former are presented.

5 **S1 Comparison with biomass and ZSS climatology
6 of A22**

- 7 It is observed that D215 is shallower at all locations and as a result a lower biomass and
8 ZSS as seen in the climatology of the present study (Fig. S1). The difference in D215 is
9 prominent off Goa; while in the previous climatology the D215 is deeper and lies along
10 D23, in the present climatological data the D215 is shallower and lies ~20–40 m above
11 the D23 during January to April. A relatively lower biomass is present above z215 year
12 round which reflects in overall lower ZSS of Goa and Mumbai. In the present data, the
13 ZSS maximum off Mumbai occurs in March instead of February (A22), due to a lower
14 ZSS value. The second maximum occurs in August and is less pronounced in recent data
15 (Fig. S1 d1, d2). There is dramatic decrease in the minimum off Mumbai that occurs in
16 October and ZSS increases rapidly afterwards till February, and the minor peak seen in
17 A22 is not observed off Mumbai. Off Kollam, higher biomass occurs from May to June in
18 A22, and from May to June and September to November in the present study, with a ZSS
19 minimum in August. The higher ZSS on either side to this minimum is less pronounced
20 in A22. This difference in ZSS with regard to A22 is clearly seen in the correlation of
21 A22 and present ZSS climatology, which is 0.60 off Kollam, 0.94 off Mumbai, and 0.98 off
22 Goa. In the present study, chl-a biomass peaks across all locations in August, and a minor
23 peak off Mumbai. Off Kollam, a zooplankton-phytoplankton relationship discrepancy is
24 consistent with A22 findings. The climatological values of chl-a and ZSS is depicted in
25 Table S1.

26 **S2 Variability and analysis techniques**

27 **S2.1 Interannual, annual, and intra-annual variability**

28 The mean biomass, standard deviation at 40 m and 104 m, and the surface-to-deep
29 biomass difference is presented in Table S2. Biomass time series exhibit variability across
30 distinct temporal bands, from daily to multi-year scales. The most fundamental is diel
31 vertical migration, with higher biomass at depth during the day and near the surface at
32 night.

33 On longer timescales, interannual variability arises due to changes in monsoon-driven
34 upwelling. This variability appears in two forms: (1) quasi-periodic changes with periods
35 > 400 days, evident in the wavelet power (\sim 600–800 days) off Mumbai, Goa, and Kollam
36 (Fig. 9), and (2) aperiodic deviations from the typical seasonal cycle (Fig. 5).

37 Annual variability (300–400 days) reflects seasonal shifts (Fig.S2, left), while intra-
38 annual variability (100–250 days) captures transitions between seasons. At the NEAS,
39 both summer and winter monsoons drive chl-*a* blooms, but asymmetries in wind forcing
40 lead to a stronger semi-annual cycle (Jensen, 1993; Schott and McCreary, 2001) (Fig. S2,
41 right; Section 3.2). Intraseasonal variability (5–90 days) stems from short-term environ-
42 mental changes (Fig. 11), with biomass bursts lasting from a few days to several weeks,
43 often coinciding with mesoscale current activity (Amol et al., 2014; Chaudhuri et al.,
44 2020) (Section 5).

45 In annual-band plots, contours of biomass peaks often tilt upward, indicating upward
46 phase propagation. While less pronounced than in the annual WICC cycle (Amol et al.,
47 2014; Chaudhuri et al., 2020, 2021), this tilt suggests physical–biological coupling. It
48 occurs intermittently across all variability bands and results in phase differences between
49 surface and deep biomass time series. In-phase signals at both depths yield higher or
50 lower column-integrated biomass (e.g., Oct–Nov 2019; Fig.S3), while phase offsets (e.g.,
51 Mar–May 2019) lead to subdued values. Such phase lags between depths or moorings
52 can be further analyzed via wavelet coherence (Section S2.2.1).

53 **S2.2 Wavelet analysis and filtering methods**

54 It is essential to first understand Fourier analysis before we discuss wavelet analysis.
55 Fourier analysis decomposes a time series into a sum of sine and cosine functions. The
56 resulting power spectrum reveals peaks that correspond to the dominant periods or fre-
57 quencies within the signal. This approach is particularly effective for analyzing signals
58 with known periodic components, such as annual (360 days) and semi-annual (180 days)
59 cycles with fixed periodicity.

60 Fourier analysis can obscure the non-stationary signals of a time series and can mis-
61 represent the power at a given period. However, real world cases includes non-stationary
62 signals and therefore wavelet analysis is needed to deal with time series data (Torrence
63 and Compo, 1998; Maraun and Kurths, 2004) as it provides a representation of time
64 series in time-frequency domain. It employs wavelets, a localized wave-like functions that
65 can be customized by varying wavelet’s scale and position along the time series to iden-
66 tify periodic (stationary) and irregular (non-stationary) patterns and their strength with
67 time. This analysis is routinely used in time series data in the field of oceanography and
68 geophysics, biomedical engineering and signal processing etc.

69 **S2.2.1 Wavelet analysis**

70 Wavelet analysis has a crucial role to identify the periods of variability whether they
71 are continuous round the year as in the annual cycle or discrete bursts that shows up in
72 spectra within the intraseasonal band. Biomass time series at 40 and 104 m is chosen and
73 decomposed to time (abscissa) vs frequency (ordinate) domain (Fig. 6). The horizontal
74 lines extending from the ordinate indicate specific periods. The color intensity along each
75 line in the wavelet spectrum reflects the strength and persistence of the corresponding
76 periodic signal over time. Two additional features should be noted: 1) the cone of
77 influence (CoI), which delineates regions where edge effects caused by the finite length of
78 the time series may distort the spectral power; and 2) contours of statistical significance,
79 which highlight regions of the spectrum where the detected features are unlikely to be
80 due to random variability. A feature must be within the CoI and statistically significant
81 to make correct interpretation on the observed variability in the time series. For example,
82 at the annual scale (365 days) off Mumbai (Fig. 6), intensity of wavelet spectra is high,
83 it lies well within CoI, and is statistically significant. The semi-annual cycle is seen along
84 with bursts in intraseasonal time scales.

85 Wavelet coherence builds upon the continuous wavelet transform, allowing for the
86 analysis of non-stationary signals. While correlation gives a static information about the
87 overall relationship between two variables, wavelet coherence normalises the cross wavelet
88 spectrum by their respective wavelet power spectra resulting in a coherence measure that
89 ranges from 0 (no correlation) to 1 (perfect correlation) along the time series for any
90 given period. Though comparison of spectra between periods within a narrow band is
91 permissible at higher periods, cross period comparison can't be made beyond a certain
92 ord due to emphasis of normalization on wavelet power at higher period (Maraun and
93 Kurths, 2004). This is where filtering techniques are applied to compare the strength of
94 variability across different frequency bands.

95 **S2.2.2 Filtering method**

96 Filtering is a signal processing method used to isolate variability within a specific fre-
97 quency band by suppressing signals outside that range. The Lanczos filter, commonly
98 used for this purpose, effectively reduces spectral leakage while preserving the signal of
99 interest (Duchon, 1979). A shortcoming of filtering method is loss of data at the begin-
100 ning and end of time series depending on the length of filtering window. While wavelet
101 analysis captures how variability evolves across all timescales, Lanczos filtering focuses
102 on fluctuations within a selected band, enabling direct comparisons between frequency
103 bands (Table S3, S4, Figs. S4–S9). Note that the negative (positive) numbers in filtered
104 biomass is representing deviation i.e., decrease (increase) from the mean.

105 **S3 Quality control tests for Kollam (2020)**

106 The interannual variability appears particularly strong off Kollam, indicating uncertainty
107 about potential data quality issues. To investigate this, the following analyses were
108 conducted on the 2019–2020 biomass dataset from the Kollam: 1) assessment of pre-
109 deployment tests and base echo intensity (Er) prior to deployment in 20 October 2019,
110 2) comparison between in-situ MPN biomass and corresponding backscatter values post
111 deployment.

112 The first analysis assesses the sensitivity accuracy of the ADCP instrument (Fig. S10,
113 top panel). Given that the ADCP was retrieved and redeployed, its baseline echo intensity
114 is expected to remain stable across servicing. However, following its redeployment on
115 20 October 2019 off Kollam, the initial reference profile used to establish the base echo in-
116 tensity showed anomalously high values. This indicated an apparent drop in backscatter,
117 raising concerns regarding possible calibration, sensitivity, or deployment-related incon-
118 sistencies.

119 To further investigate, the second analysis examined in-situ biomass samples collected
120 post-deployment from the same region. These samples supported the backscatter observa-
121 tions: measured biomass was notably lower and deviated beyond one standard deviation
122 from the least-squares biomass–backscatter regression line. This alignment strengthens
123 the case for a real reduction in biomass rather than an instrumental error (Fig. S10,
124 bottom panel). At the same time, it underscores the importance of in-situ sampling in
125 validating long-term ADCP-derived observations. Without these direct measurements,
126 confidence in a year-long deployment would be limited. In this instance, low backscat-
127 ter coincides with genuinely low biomass, demonstrating the complementary value of
128 both approaches. The evaluation of backscatter and biomass before retrieval and af-
129 ter deployment highlights the critical role of in-situ biomass measurements in validating
130 backscatter-derived biomass estimates.

131 **S4 Caveats and strengths of ADCP backscatter as a 132 proxy for zooplankton biomass**

133 To investigate seasonal variability in zooplankton abundance in the Arabian Sea, the
134 JGOFS program conducted three cruises during distinct seasons: inter-monsoon (Apr–May
135 1994), winter (Feb–Mar 1995), and summer (Jul–Aug 1995), with sampling conducted
136 twice daily (midday and midnight) at each station (Madhupratap et al., 1996). However,
137 using just two temporal snapshots to represent an entire season may not adequately cap-
138 ture the dynamic nature of zooplankton biomass. The spatial map of mesozooplankton
139 distribution, such as the one by Jyothibabu et al. (2010) for each season (see Fig. 11
140 of Jyothibabu et al. (2010)) is limited by sampling frequency and time elapsed to cover
141 stations, and the measured biomass is prone to distortion.

142 Consider the summer monsoon months off Mumbai during early June of 2019 (Fig. 10),
143 where a spike in biomass is observed due to an instantaneous increase in the high-
144 frequency components of biomass variability, resulting in an increase of $\sim 150 \text{ mg m}^{-3}$
145 within a few days. Similar spikes are seen at other locations too, e.g., off Kollam during
146 the end of July and multiple instances in September of 2019. These spikes last only for a
147 day to a few days, but the bursts in biomass tend to last longer, from a few days to a few
148 weeks. This burst is also observed off Kollam, Udupi, and Goa, albeit with decreasing
149 intensity as we go poleward (Fig. 10, Table S2). Such coherency can only be observed if
150 continuous and frequent measurements were taken across EAS. These limitations high-
151 light the need for high-resolution, continuous observations, such as those provided by
152 ADCP backscatter, to accurately assess zooplankton variability in time and space.

153 **References**

- 154 P. Amol, D. Shankar, V. Fernando, A. Mukherjee, S. G. Aparna, R. Fernandes, G. S.
155 Michael, S. T. Khalap, N. P. Satelkar, Y. Agarvadekar, M. G. Gaonkar, A. P. Tari,
156 A. Kankonkar, and S.P. Vernekar. Observed intraseasonal and seasonal variability of
157 the West India Coastal Current on the continental slope. *J. Earth Syst. Sci.*, 123(5):
158 1045–1074, 2014. doi: 10.1007/s12040-014-0449-5.
- 159 S. G. Aparna, D. V Desai, D Shankar, A. C Anil, Shrikant Dora, and R. R. Khedekar.
160 Seasonal cycle of zooplankton standing stock inferred from ADCP backscatter mea-
161 surements in the eastern Arabian Sea. *Prog. Oceanogr.*, 203:102766, 2022. doi: 10.1016/
162 j.pocean.2022.102766.
- 163 Anya Chaudhuri, D. Shankar, S. G. Aparna, P. Amol, V. Fernando, A. Kankonkar, G. S.
164 Michael, N. P. Satelkar, S. T. Khalap, A. P. Tari, M. G. Gaonkar, S. Ghatkar, and R. R.
165 Khedekar. Observed variability of the West India Coastal Current on the continental
166 slope from 2009–2018. *J. Earth Syst. Sci.*, 129(1):57, 2020. doi: 10.1007/s12040-019-
167 1322-3.
- 168 Anya Chaudhuri, P Amol, D Shankar, S Mukhopadhyay, S. G Aparna, V Fernando,
169 and A Kankonkar. Observed variability of the West India Coastal Current on the
170 continental shelf from 2010–2017. *J. Earth Syst. Sci.*, 130:1–21, 2021. doi: 10.1007/
171 s12040-021-01603-4.
- 172 Claude E Duchon. Lanczos filtering in one and two dimensions. *J. Appl. Meteorol.
173 Climatol.*, 18(8):1016–1022, 1979. doi: 10.1175/1520-0450(1979)018<1016:LFIOAT>2.
174 0.CO;2.
- 175 Tommy G Jensen. Equatorial variability and resonance in a wind-driven Indian Ocean
176 model. *J. Geophys. Res. Oceans*, 98(C12):22533–22552, 1993. doi: 10.1029/93JC02565.
- 177 R Jyothibabu, N. V Madhu, H Habeebrehman, K. V Jayalakshmy, K. K. C Nair, and C. T
178 Achuthankutty. Re-evaluation of ‘paradox of mesozooplankton’ in the eastern Arabian
179 Sea based on ship and satellite observations. *J. Mar. Syst.*, 81(3):235–251, 2010. doi:
180 10.1016/j.jmarsys.2009.12.019.
- 181 M Madhupratap, T. C Gopalakrishnan, P Haridas, K. K. C Nair, P. N Aravindakshan,
182 G Padmavati, and Shiney Paul. Lack of seasonal and geographic variation in mesozoo-
183 plankton biomass in the Arabian Sea and its structure in the mixed layer. *Curr. Sci.*,
184 71(11):863–868, 1996. URL drs.nio.org/drs/handle/2264/2154.
- 185 Douglas Maraun and Jürgen Kurths. Cross wavelet analysis: significance testing and
186 pitfalls. *Nonlin. Processes Geophys.*, 11(4):505–514, 2004. doi: 10.5194/npg-11-505-2004.
- 187 Friedrich A. Schott and Julian P. McCrea. The monsoon circulation of the Indian
188 Ocean. *Prog. Oceanogr.*, 51(1):1–123, 2001. ISSN 0079-6611. doi: 10.1016/S0079-
189 6611(01)00083-0.
- 190 Christopher Torrence and Gilbert P Compo. A practical guide to wavelet analysis. *Bull.
191 Am. Meteorol. Soc.*, 79(1):61–78, 1998. doi: 10.1175/1520-0477(1998)079<0061:APGTWA>
192 2.0.CO;2.

Table S1:

The climatological mean, standard deviation, and range of ZSS (g m^{-2}) and chl-*a* (mg m^{-3}) are presented for seven locations. The standard deviation indicates the spread of values for each variable, while the range represents the difference between the peak and minimum values.

Mooring location	Chlorophyll			ZSS		
	Mean	SD	Range	Mean	SD	Range
Okha	0.51	0.24	0.72	20.5	1.8	5.8
Mumbai	0.33	0.13	0.39	23.6	2.6	8
Jaigarh	0.27	0.05	0.15	24.2	2.9	9
Goa	0.28	0.15	0.55	21.2	1.9	6.3
Udupi	0.59	0.56	1.54	21.9	1.9	5.8
Kollam	0.64	0.7	2.26	24.6	1.1	4.1
Kanyakumari	0.61	0.52	1.62	20.1	0.6	2.4

Table S2:

The mean and standard deviation of zooplankton biomass (mg m^{-3}) at 40 m and 104 m across seven mooring sites are tabulated based on the corresponding *daily data*. The last column represents the biomass range, calculated as the difference between the mean at 40 m and that at 104 m.

Mooring location	40 m biomass		104 m biomass		Decrease with depth (40 m - 104 m)
	Mean	SD	Mean	SD	
Okha	212.8	27.5	143.6	29.7	69.2
Mumbai	248.6	37.2	169.8	34.6	78.8
Jaigarh	253.5	38.2	170.4	50	83.1
Goa	216.3	35	153.5	37.2	62.8
Udupi	227.6	39.7	158.8	38.4	68.8
Kollam	247.9	55.5	184.2	48.3	63.7
Kanyakumari	192.3	34.4	157.5	23.8	34.8

Table S3:

Standard deviation of distinct variability components of 40 m biomass at each location, with corresponding 104 m biomass variability shown in brackets (units: mg m^{-3}). The first column represents the variance associated with the seasonal cycle, combining variability from the annual and intra-annual bands. Notably, the intraseasonal variability (5–90 days) is comparable to, and at some locations exceeds, the seasonal variability, indicating stronger fluctuations occurring within a season.

Mooring location	Seasonal (100-400 days)	Annual (300-400 days)	Intra-annual (100-250 days)	Intraseasonal (5-90 days)
Okha	6.3 (14.2)	2.3 (2.5)	4.9 (10.1)	17.7 (16.7)
Mumbai	19.1 (19.4)	5.6 (5.8)	13.2 (12.7)	20.2 (19.8)
Jaigarh	14.4 (20.9)	5.4 (7.9)	12.1 (12)	21.1 (23.8)
Goa	16.2 (17.8)	2.9 (6.5)	12.3 (10.1)	20.2 (17)
Udupi	22.1 (25)	4.9 (8.3)	15.2 (15.1)	23.7 (15.5)
Kollam	24.3 (15.6)	6.5 (5.1)	18.4 (10.9)	26.7 (17.4)
Kanyakumari	14.1 (9)	3.8 (3.4)	10 (5.6)	21.2 (14.3)

Table S4:

Standard deviation of distinct variability components of ZSS and chl- a computed from their respective daily data. Units are mg m^{-2} for ZSS and mg m^{-3} for chl- a (in parentheses). The first column represents the variance associated with the seasonal cycle, combining variability from the annual and intra-annual bands. For Mumbai and Jaigarh, chl- a data are only available for the intraseasonal band due to the infeasibility of applying filtering methods to discontinuous and unevenly spaced data over longer time records.

Mooring location	Seasonal (100-400 days)	Annual (300-400 days)	Intra-annual (100-250 days)	Intraseasonal (5-90 days)
Okha	0.7 (0.3)	0.2 (0.1)	0.5 (0.2)	1.1 (0.4)
Mumbai	1.6 (–)	0.5 (–)	0.9 (–)	1.2 (0.1)
Jaigarh	1.9 (–)	0.7 (–)	0.9 (–)	1.4 (0.1)
Goa	1.5 (0.1)	0.4 (0)	1 (0.1)	1.1 (0.1)
Udupi	1.8 (0.5)	0.3 (0.1)	1.3 (0.3)	1.2 (0.7)
Kollam	1 (0.6)	0.1 (0.2)	0.9 (0.5)	1.5 (0.7)
Kanyakumari	0.7 (0.5)	0.2 (0.1)	0.5 (0.3)	1.3 (0.7)

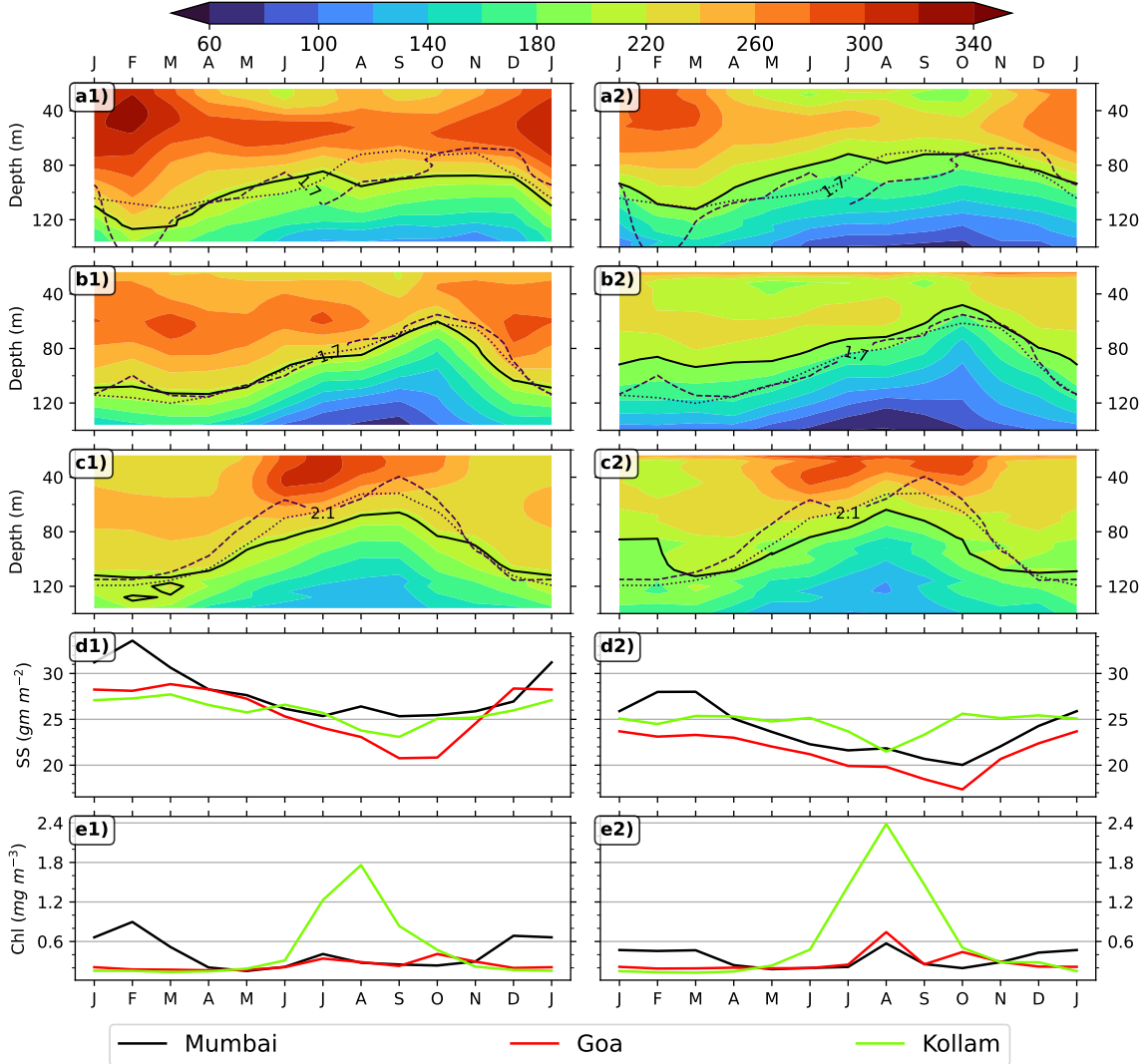


Figure S1: Monthly climatology of zooplankton biomass is shown in the left panels for three locations previously analyzed in (Aparna et al., 2022), with D215 represented by the solid black line. The dashed line indicates the 23°C isotherm depth, and oxygen contours are shown as dotted lines. Panels a1, b1, and c1 correspond to Mumbai, Goa, and Kollam, respectively. Panel d1 shows the ZSS climatology (integrated over 24–140 m), and panel e1 shows the chl- a climatology. The right panels are based on data from 2017 to 2023.

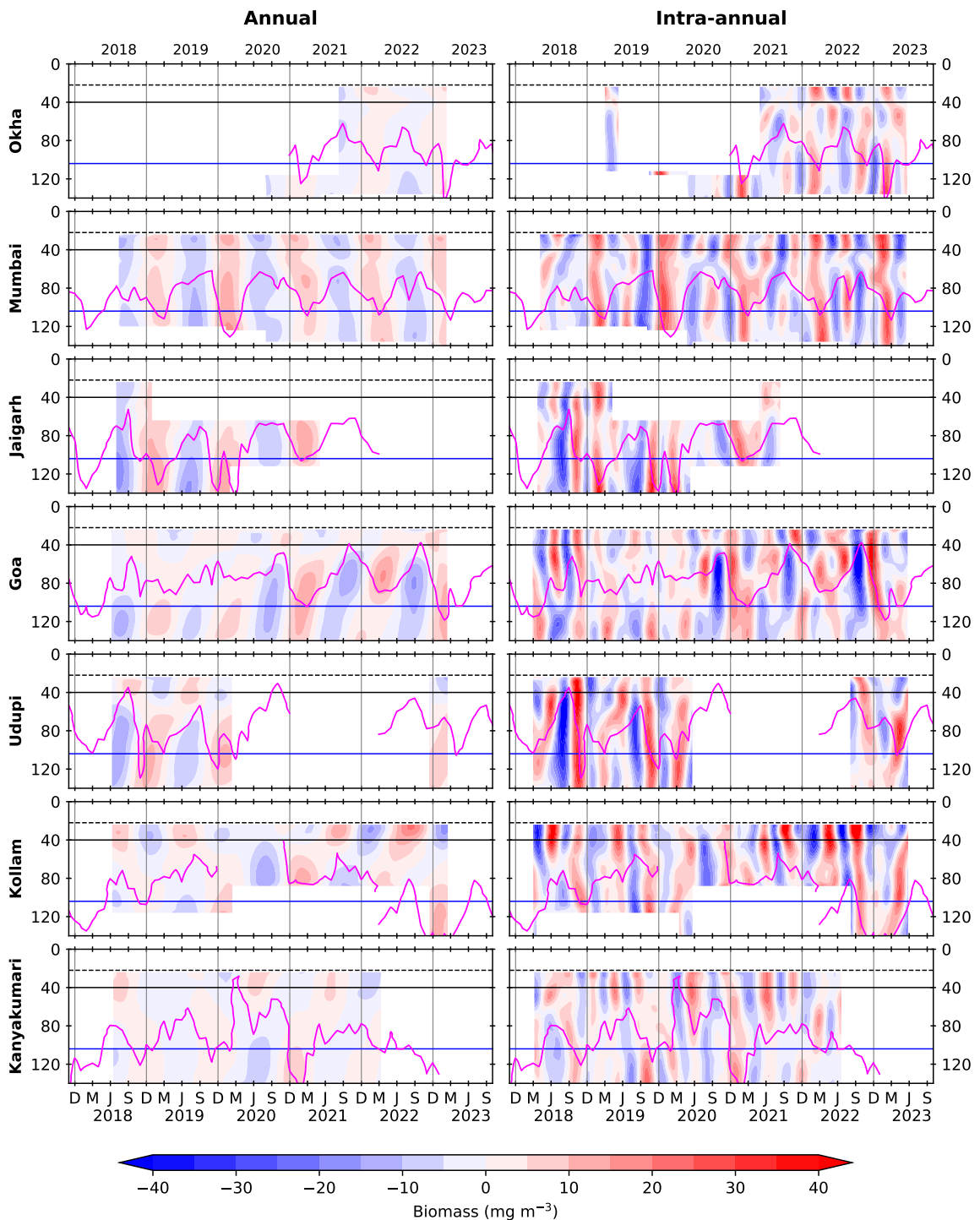


Figure S2: Biomass variability in the annual (300–400 days) and intra-annual (100–250 days) bands is extracted using a band-pass filter. Horizontal black and blue lines represent 40 m and 104 m depths, respectively; vertical black lines separate the years. The dashed line at 22 m marks the upper edge of the first bin (i.e., 24 m), and the solid magenta curves denote D215 (or D175 off Okha and Kanyakumari), derived from the monthly biomass time series.

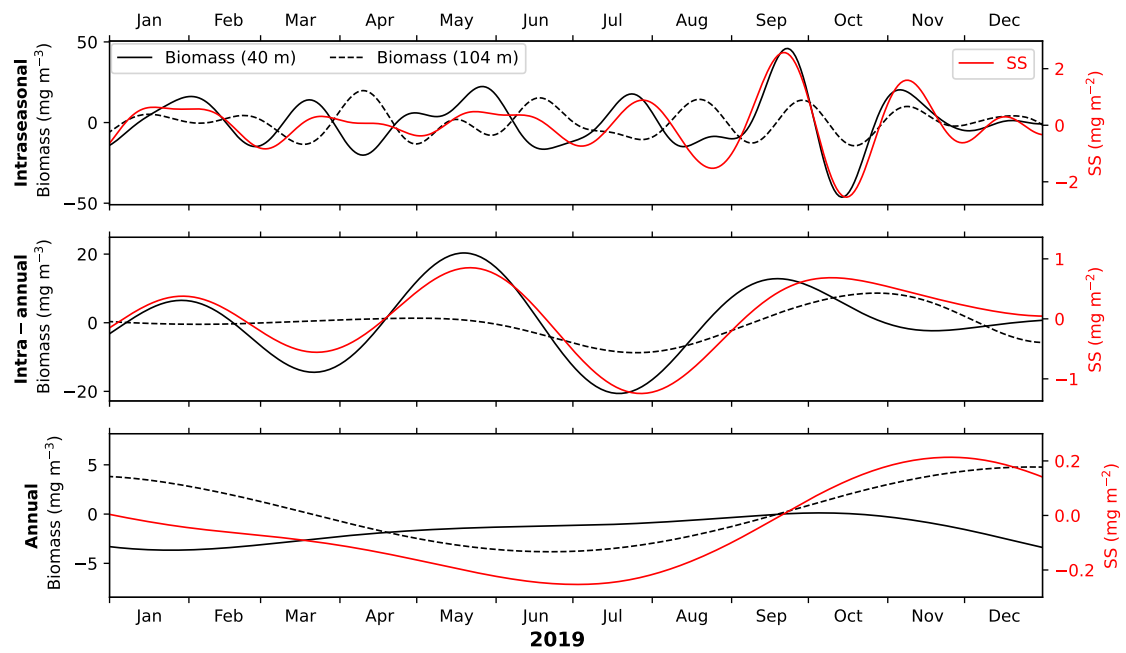


Figure S3: Comparison of biomass at 40 m and 104 m with ZSS (column-integrated standing stock, 24–120). Biomass at 104 m may or may not be in phase with upper-ocean biomass at 40 m, thereby enhancing or dampening ZSS variability. This behavior is evident across all distinct bands of variability.

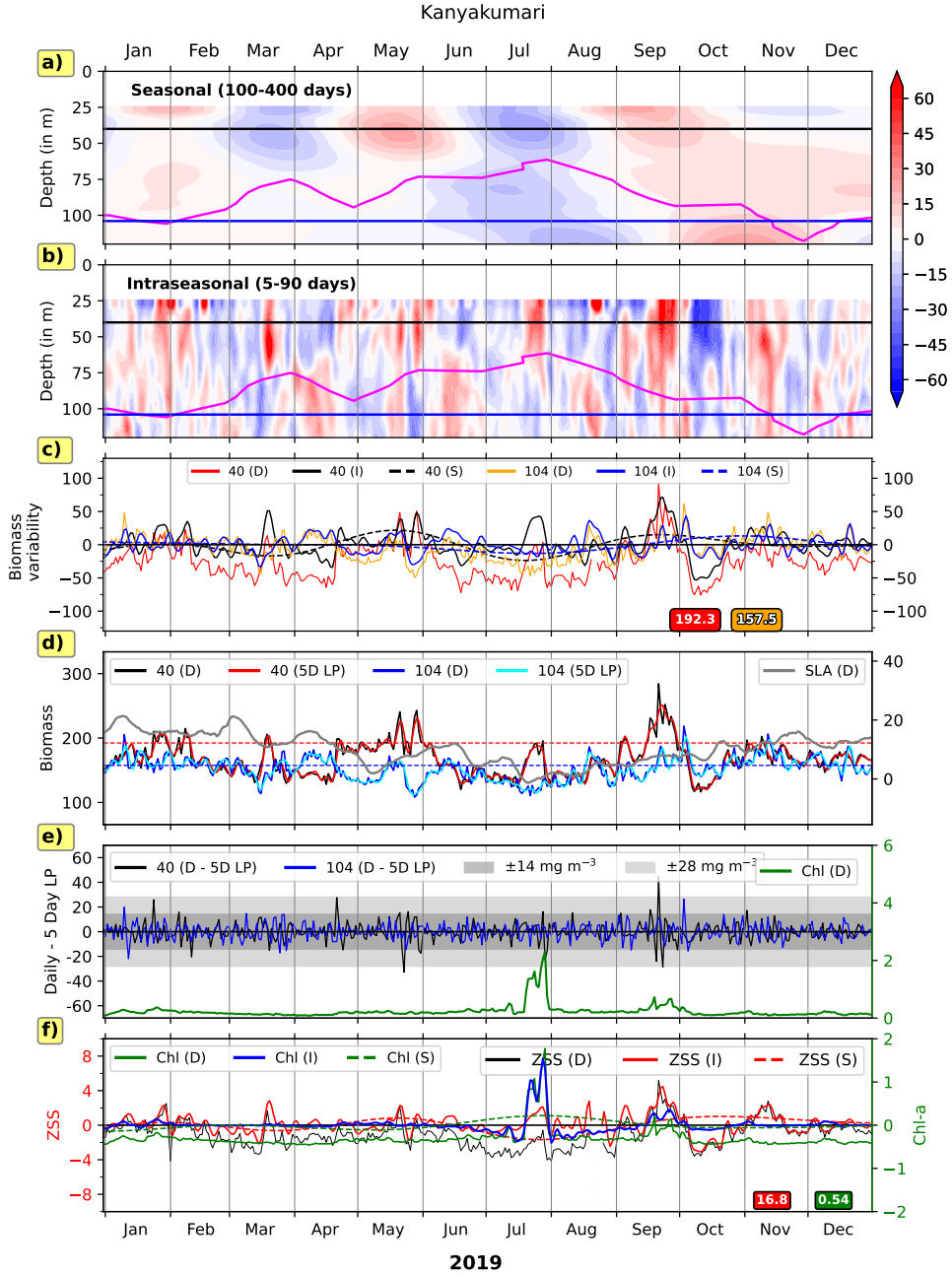


Figure S4: Panels show a comparison of biomass variability in the seasonal and intraseasonal bands off Kanyakumari. The top two panels present time-depth plots of seasonal and intraseasonal biomass on the same scale. Biomass at 40 m and 104 m is marked by black and blue lines, respectively; vertical grey lines separate months, and the magenta curve denotes D175. The third panel shows daily, intraseasonal (5–90 days), and seasonal (100–400 days) biomass at 40 m and 104 m, with the mean daily biomass indicated in the bottom right corner. The fourth panel displays daily biomass overlaid with 5-day low-pass filtered biomass and daily SLA. Notably, high (low) SLA corresponds to lower (higher) biomass at 40 m. The fifth panel shows the difference between daily and 5-day low-pass filtered biomass at both depths. Grey and light grey shaded regions denote the 1 SD and 2 SD bounds from the backscatter–biomass relationship, onto which daily chl-*a* is overlaid. The bottom panel shows chl-*a* and ZSS variability in the intraseasonal and seasonal bands.

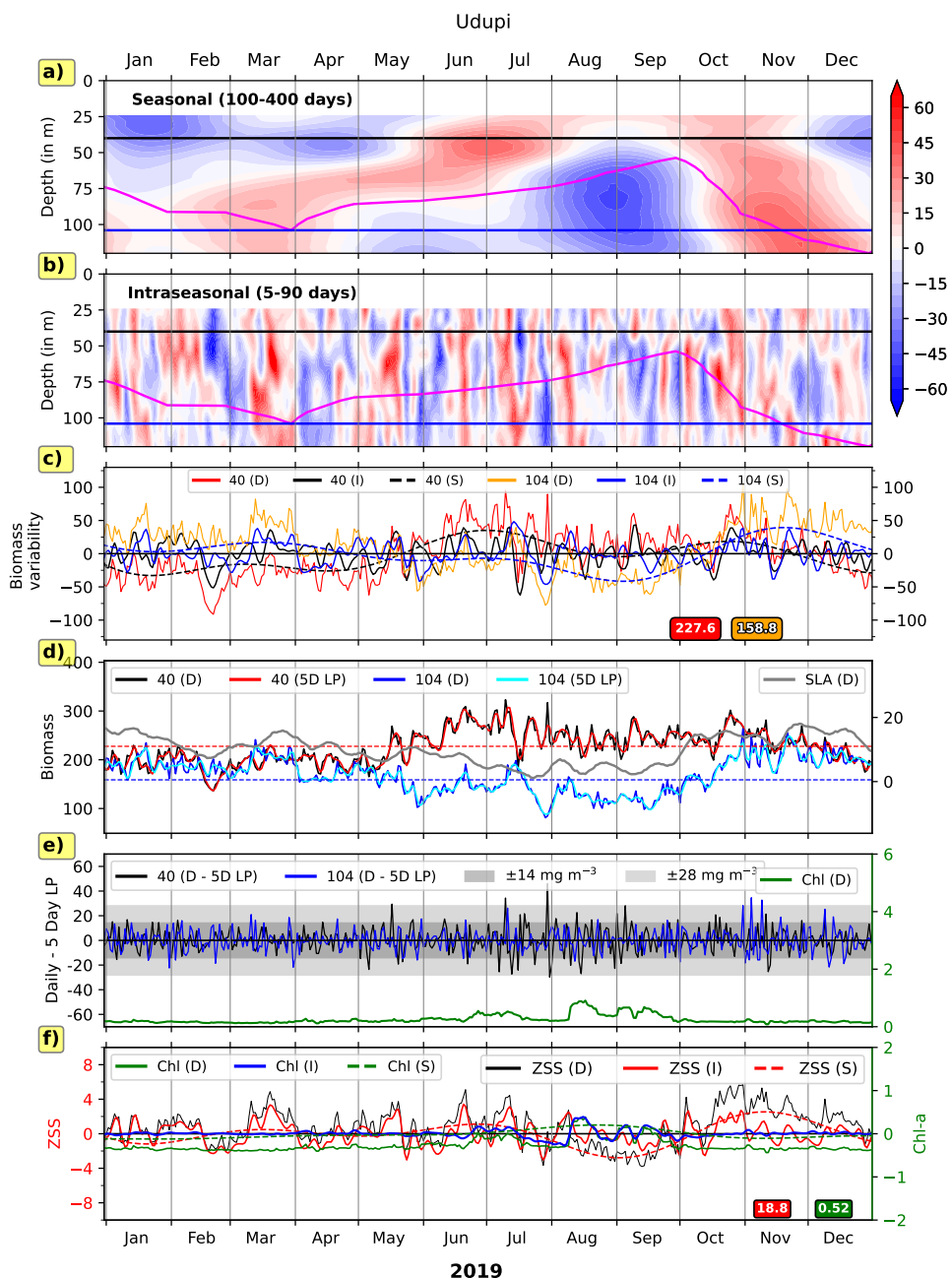


Figure S5: Same as in Fig. S4 but for Udupi with D215 curve in top two panels.

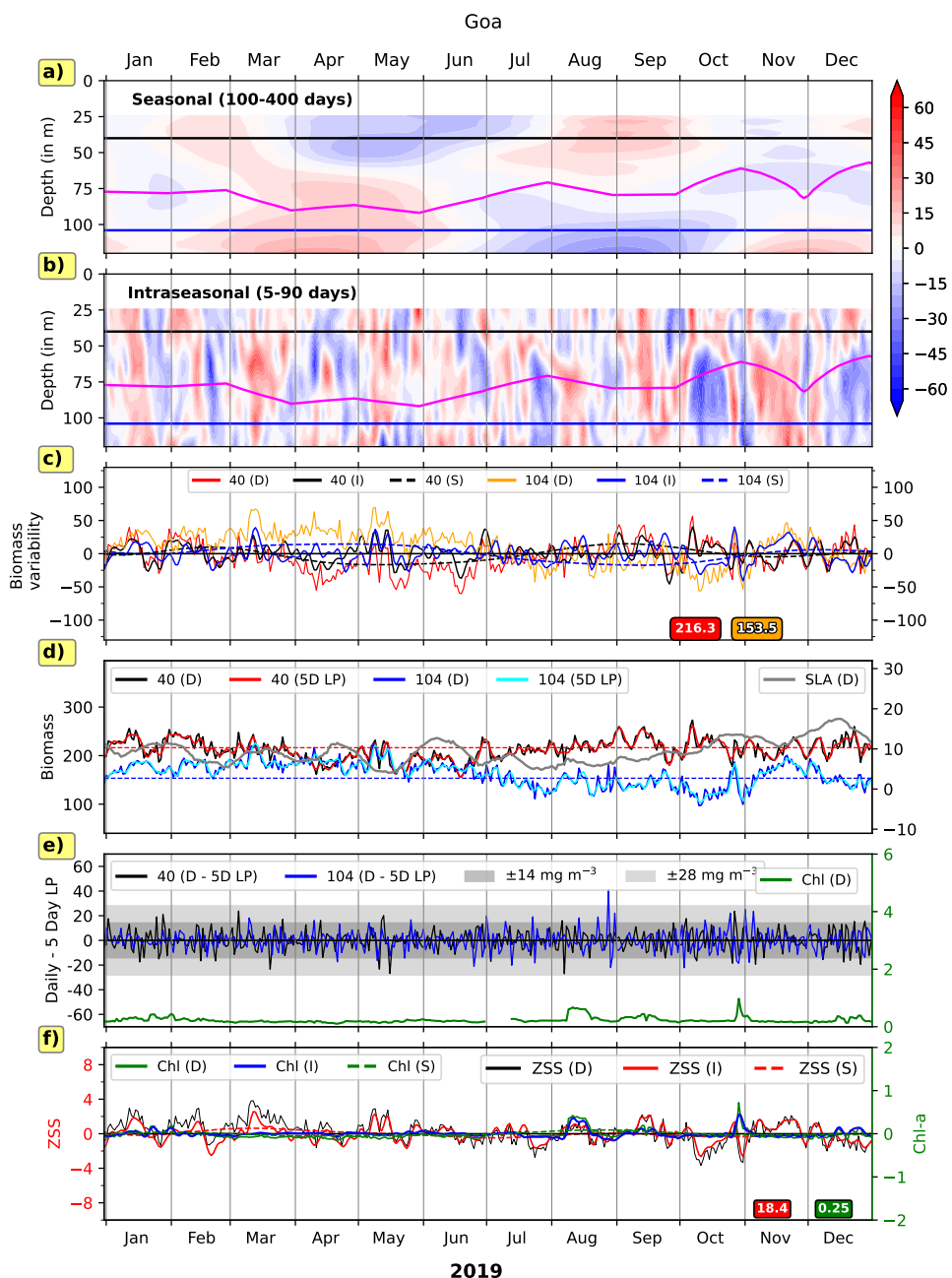


Figure S6: Same as in Fig. S4 but for Goa with D215 curve in top two panels.

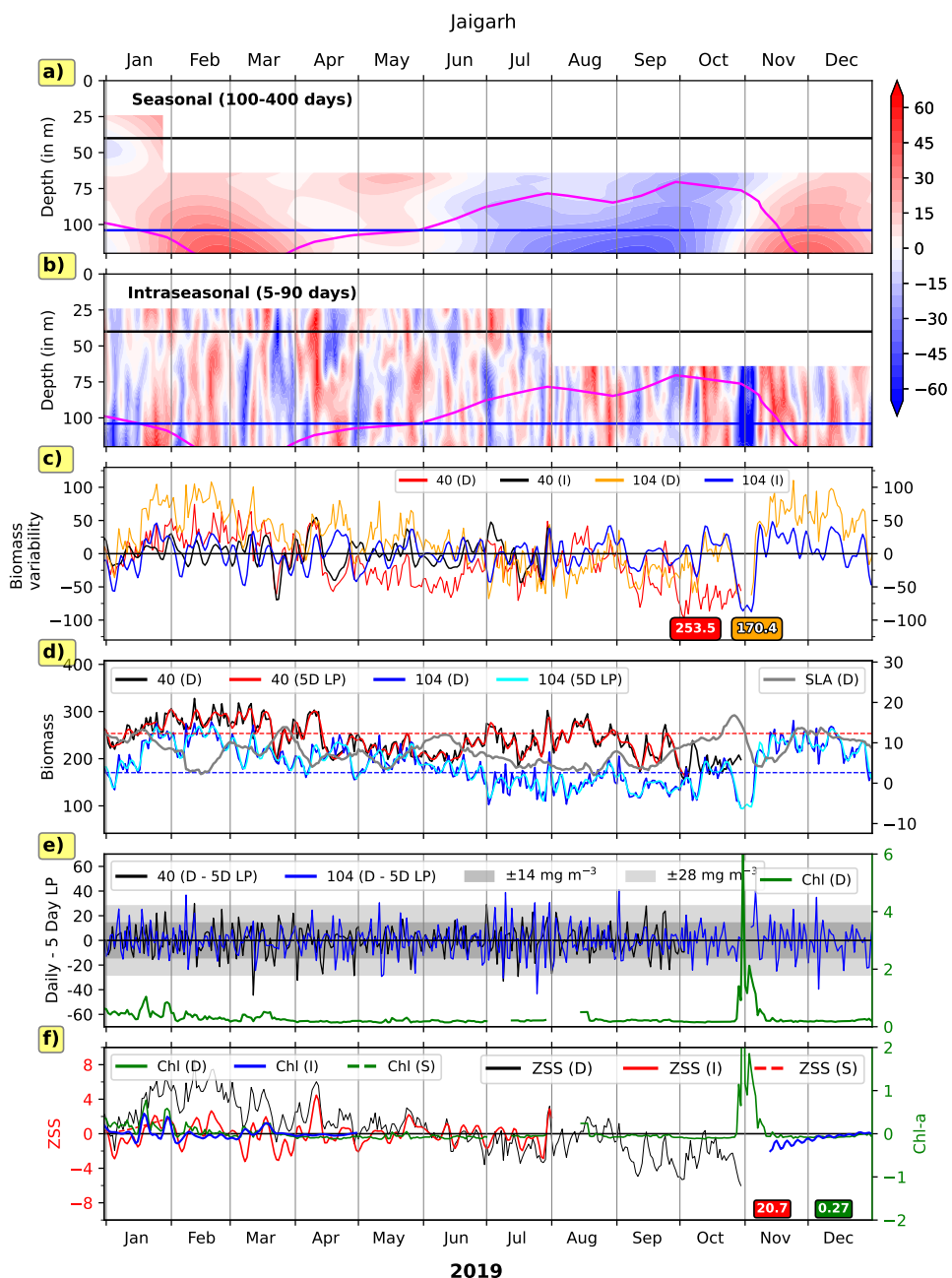


Figure S7: Same as in Fig. S4 but for Jaigarh with D215 curve in top two panels.

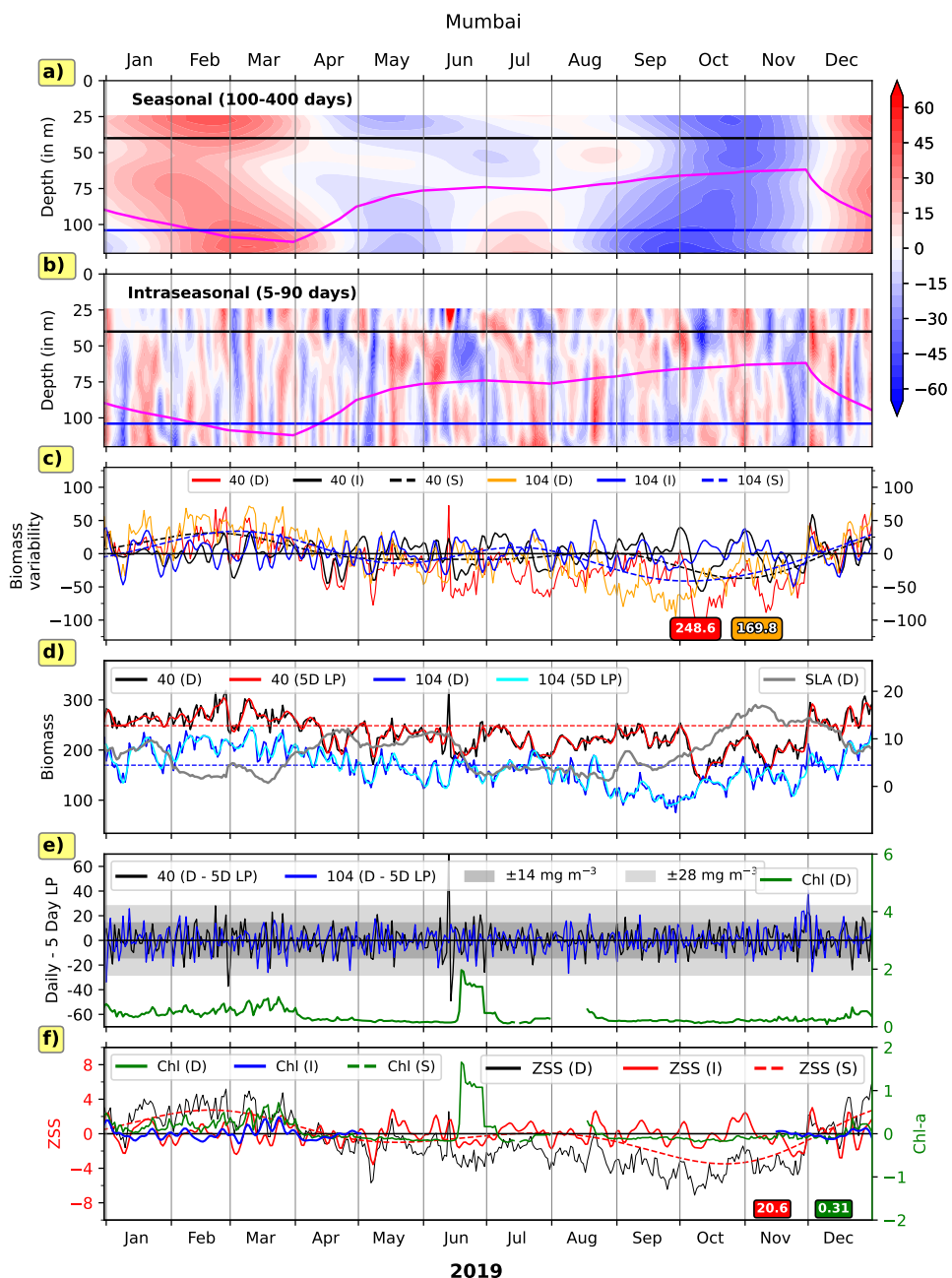


Figure S8: Same as in Fig. S4 but for Mumbai with D215 curve in top two panels.

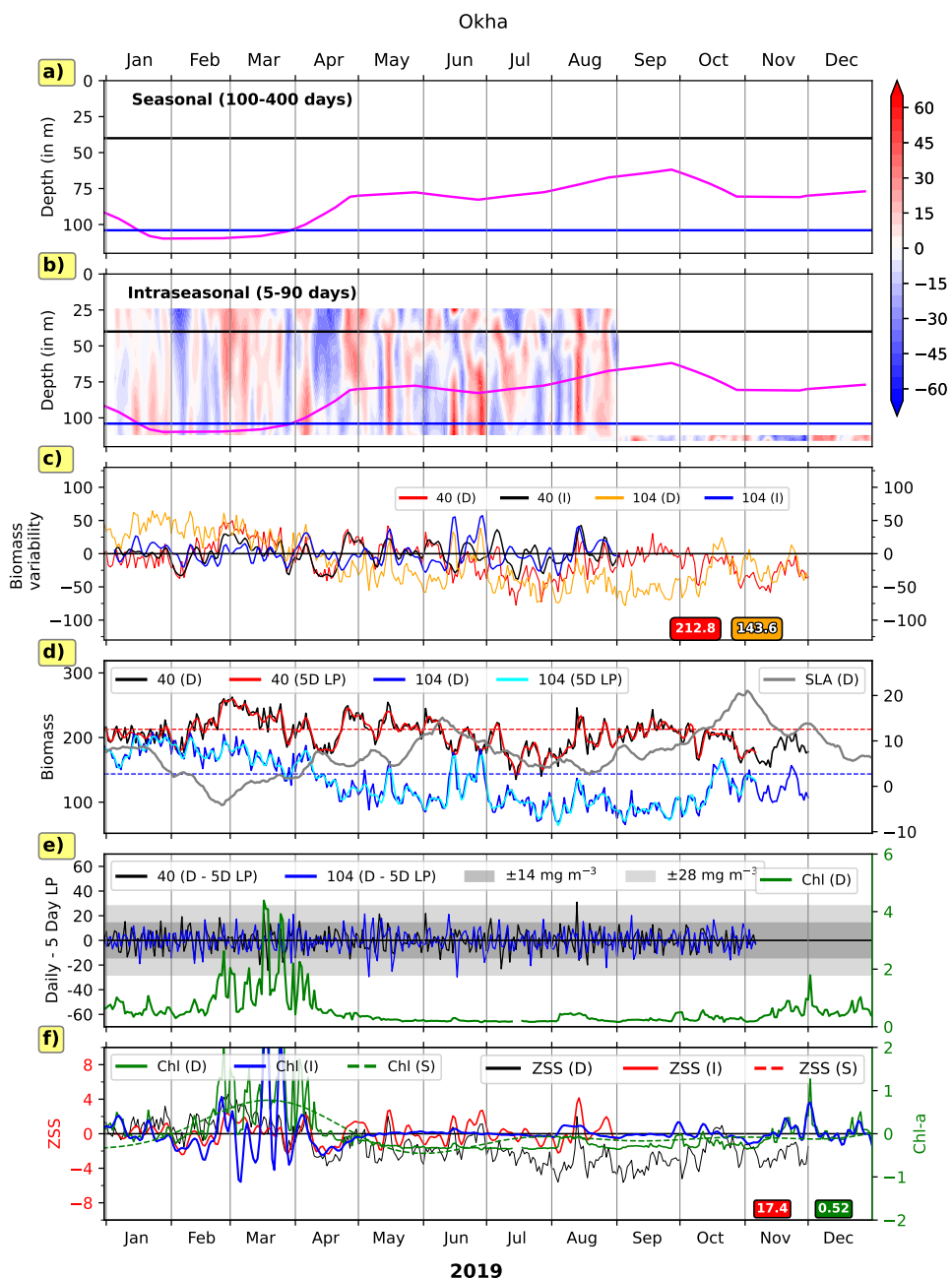


Figure S9: Same as in Fig. S4 but for Okha with D175 curve in top two panels.

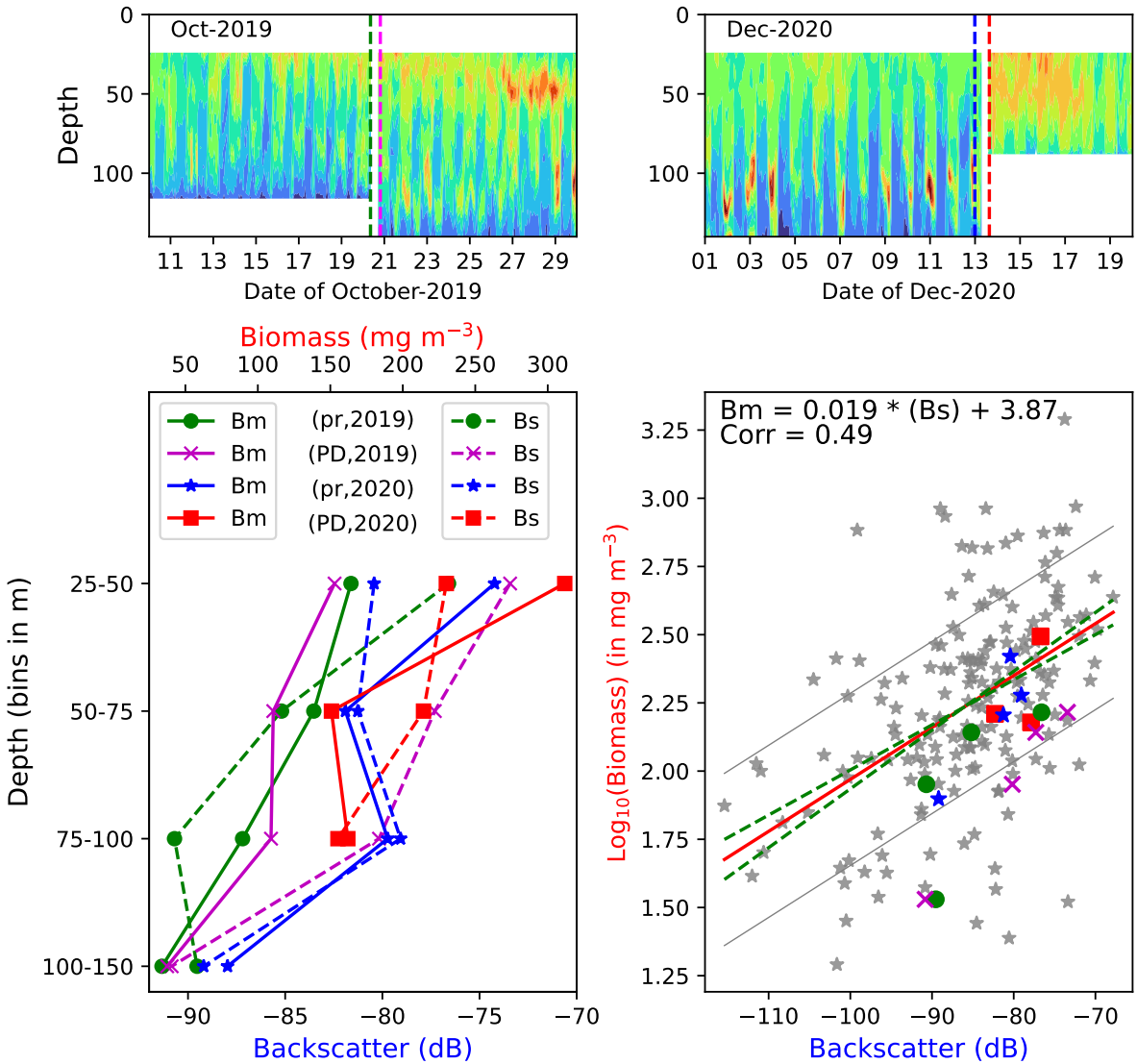


Figure S10: The top left panel shows data from October 2019, with retrieval and redeployment marked by dashed green and dashed purple lines, respectively. The top right panel shows data from December 2020, with retrieval in dashed blue and redeployment in dashed red. The bottom left panel presents in-situ biomass profiles (Bm) as solid lines and corresponding backscatter profiles (Bs) as dashed lines for the pre-retrieval (PR) and post-deployment (PD) phases of 2019 and 2020. The bottom right panel displays biomass (\log_{10} scale) plotted against backscatter for Kollam in 2019 and 2020, overlaid on the linear regression line fitted to all available data points. Symbols used in this panel match those in the bottom left panel.

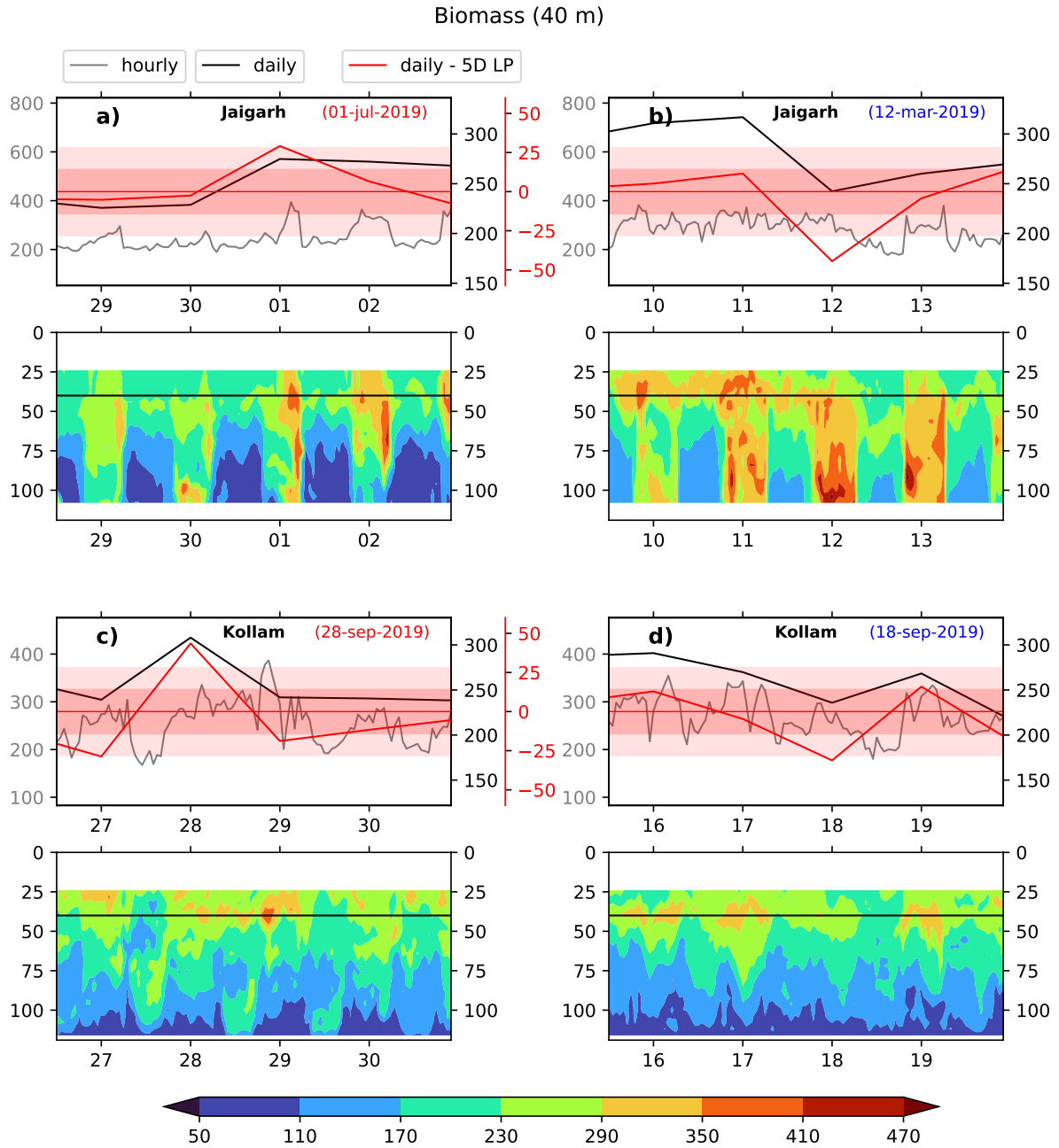


Figure S11: Spikes are shown as the difference between the mean-removed daily biomass time series (red line) and the 5-day low-pass filtered biomass (black line) at 40 m depth, off Jaigarh in panel a and b, and below it, the hourly time series illustrates the actual biomass variation throughout the day. Shaded regions represent ± 1 SD (red) and ± 2 SD (light red) from the mean-removed daily time series. The date of each spike event is noted in the top-right corner of each panel, with red and blue text indicating positive and negative spikes, respectively. Panel c and d are same but for Kollam.

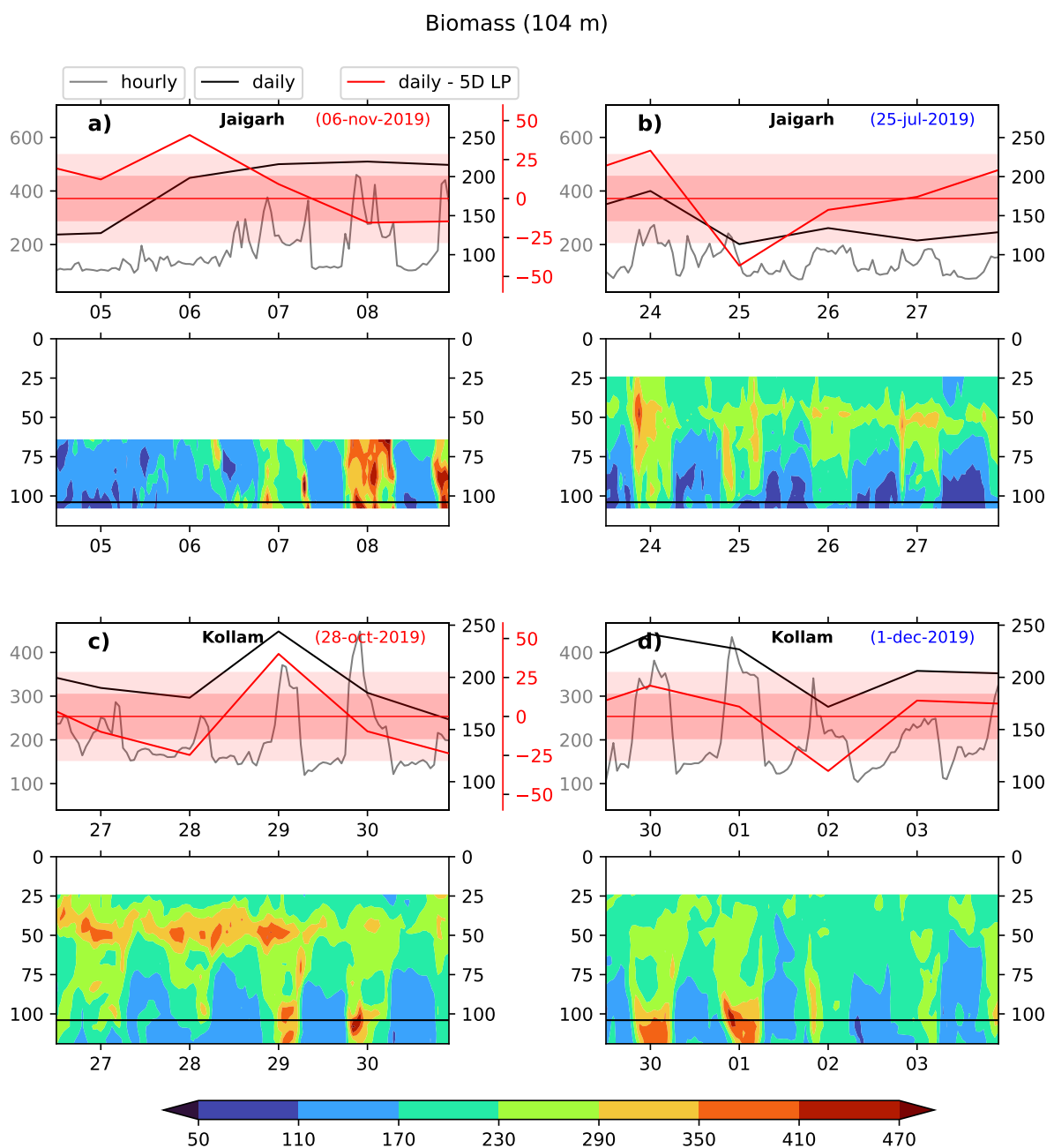


Figure S12: Same as Fig. S11 but for biomass at 104 m depth.